THE JOURNAL OF PHYSICAL CHEMISTRY C

Article

pubs.acs.org/JPCC

Nanochimneys: Topology and Thermal Conductance of 3D Nanotube–Graphene Cone Junctions

Ziang Zhang,[†] Alex Kutana,[†] Ajit Roy,[#] and Boris I. Yakobson*[,†]

[†]Department of Materials Science and Nanoengineering, Rice University, Houston, Texas 77005, United States

[#]Materials and Manufacturing Directorate, Air Force Research Laboratory, Dayton, Ohio 45433, United States

ABSTRACT: Pillared 3D carbon architectures, with the graphene layers and carbon nanotubes connected by topological junctions, have been produced and observed, as reported recently. However, the atomistic details of such junctions are hard to discern in microscopy and remain presently unclear. The simplest junction contains six heptagons in the transition region between the nanotube and graphene. Although these junctions make the pillared architectures possible, they are susceptible to failure when the whole structure undergoes mechanical or thermal stress. In this work we consider "nanochimneys", a variety of special junctions with cones in between the nanotube and graphene parts. We explore the structures of the nanochimneys (NCs) and determine their underlying topological requirements. We also study the thermal conductance of these pillared architectures and show that NCs conduct heat better than regular simple junctions.

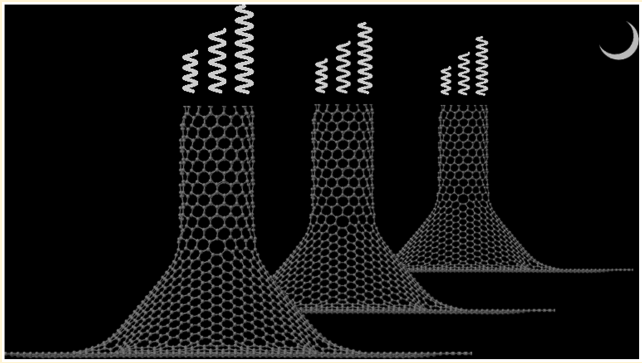

INTRODUCTION

Since its theoretical introduction in 2008 as a novel material for enhanced hydrogen storage,[1] the pillared 3D carbon architecture has become a focus of researchers' attention as one of the appealing forms of 3D carbon.[2,3] Experimental research going for its lab fabrication have met considerable success,[4−9] notably, Xue et al. developed a strategy to create 3D graphene−CNT hollow fibers with tunable dimensions.[9] Both theoretical and experimental research is ongoing to explore its potential for applications as structural materials,[10−12] supercapacitors,[8,9,13,14] hydrogen storage,[15,16] dye-sensitized solar cells,[17] and for thermal transport.[18−23]

In the majority of the experimental works, the CNT−graphene junctions are grown with chemical vapor deposition (CVD) technique.[24] The morphology of the junctions is observed in transmission electronic microscopy (TEM) images, while the connectivity between CNT and graphene is verified by measuring the electric conductivity of the whole structure. In these pillared architectures, the junction is the key component because it serves as the interface connecting the 1D and 2D building blocks. In structural applications, the junction reduces the system's mechanical strength[11] as well as affects its Poisson's ratio.[10] For hydrogen storage, the junction contains point defects that may act as adsorption sites. In thermal applications, the junction plays a key role in limiting ballistic thermal transport because of phonon-scattering effect.[19,20] Therefore, the study of junction is crucial for understanding the properties and application potential of the pillared architecture.

Although its importance is generally understood, there are few research works focused specifically on the atomistic structure of the junction. One notable effort has been made to explore the growth mechanism of the junction via molecular dynamics (MD) simulations.[25] While gaining insights on the possible growth mechanism, this work, together with other in the field, assumes there exists only one morphological type of junction: one with the CNT component directly connected to the graphene sheet. Experimental discovery of graphitic cones,[26] together with theoretical analysis of their stability,[27] however, points out to a possible alternative for constructing junctions. In this article, we provide a topological route to constructing cone junctions through nanochimneys (NCs), as well as explore its positive effect on the thermal conductance of the pillared architecture.

METHODS

Thermal conductance calculations are conducted with large-scale atomic/molecular massively parallel simulator (LAMMPS).[28,29] The atomic potential used to model carbon−carbon interaction is the adaptive intermolecular reactive bond order (AIREBO).[30] The thermal transport was simulated by using the heat flux method, in which the heat flux is induced by keeping the two ends of the system at two different temperatures using an *NVT* thermostat. The energy

Received: November 11, 2016
Revised: December 17, 2016
Published: December 21, 2016

DOI: 10.1021/acs.jpcc.6b11350
J. Phys. Chem. C 2017, 121, 1257−1262

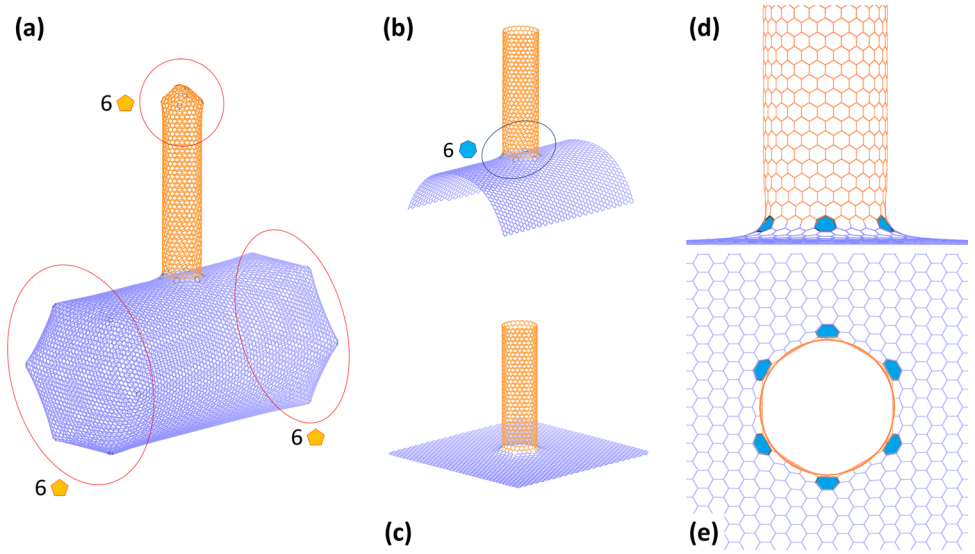

Figure 1. CNT intersection showing that there are always six heptagons in a junction. (a) A "Thor's Hammer" structure, with two capped tubes intersecting in a T shape. (b) The intersection part of the hammer structure that is topologically equivalent to a junction. (c) A CNT−graphene junction with (d) side and (e) top views showing heptagons.

added to the hot end is equal to the energy taken from the cold end, and proportional to the heat flux across the region of interest. In all calculations, systems were first thermally equilibrated, and the thermal resistance was measured for 500 ns. Various temperature differences between the two heat baths were set, varying between 20 and 125 K, yielding similar values of thermal resistance.

RESULTS AND DISCUSSION

Geometrical Connectivity of Conventional Junctions. We first look at the regular junctions connecting CNT and graphene sheets. For all of the geometries, we notice that there are six heptagons (seven-member rings) connecting the graphene sheet and the CNT, regardless of the latter's diameter or chirality (armchair, zigzag, or chiral). A natural question to be asked here would be, is this geometrical restriction the general case? Although there are plenty of works in literature that depict CNT−graphene junctions as having six heptagons, none of them, to the best of our knowledge, has considered the junction topology in great detail.

Here we demonstrate its universality. First, as a geometrical starting point, we use the formula for the number N_p of polygons with p sides in an enclosed sp^2 network,[31] as derived from the Euler equation, which can be written as

$$\sum_p (6 - p)N_p = 12 \tag{1}$$

For carbon nanostructures, p-membered atomic rings are not stable for $p \leq 4$ or $p \geq 8$; therefore, for realistic structures p can be 5, 6, or 7. In the case of $p = 6$, the term $(6 - p) = 0$. Hence eq 1 can be rewritten as

$$N_5 - N_7 = 12 \tag{2}$$

For fullerenes, regardless of the number of hexagons, there are always 12 pentagons and zero heptagons. The numbers are the same for an enclosed CNT with two caps, as topologically it is same as a fullerene. In each cap of the enclosed CNT, there are six pentagons, regardless of the size of the cap and the CNT. This fact will now be used to elaborate on the CNT−graphene junction.

Let us first look at the structure of a T-shaped tube intersection, where a smaller CNT A intersects a larger CNT B, as depicted in Figure 1. We designate then numbers of pentagons and heptagons in the intersection by the small case letters as n_5 and n_7, respectively. First assume that there are only heptagons at the junction, and all pentagons are at the three caps. Therefore, there are 18 pentagons in this structure. According to eq 2, the number of heptagons is $N_7 = 18-12 = 6$. These six heptagons are all located at the junction, so that $n_7 = N_7$, as the bulks of the two CNTs only contain hexagons. If we then allow n_5 pentagons in the junction, the total number of pentagons in the system becomes $N_5 = 18 + n_5$, and the number of heptagons at the junction is then, from the general eq 2, $n_7 = 18 + n_5 - 12 = 6 + n_5$.

Now if we take the junction part out of the intersection, we notice that it is of exactly the same structure as a CNT−graphene junction, as the graphene sheet here can be regarded as the wall of a CNT of infinite radius. Thus, we have shown that, for a CNT−graphene junction, there are always six heptagons more than pentagons independent of the sizes and chiralities of the CNTs. The relation for the numbers of heptagons and pentagons in the junction can thus be written as follows:

$$n_7 - n_5 = 6 \tag{3}$$

Dislocation Cluster as Origin of Cone on Graphene Sheet. The regular junction shown above, with all six heptagons in one plane, is not the only type of junction. Graphitic cones can be inserted between the CNT and the graphene sheet, resulting in different kinds of junctions: NCs, with different structural and thermal properties. To study the topological structure of NCs, it is helpful to look into how a cone connects to the graphene sheet, before adding the CNT into consideration.

Fitting the edge of the cone onto a hole on the graphene sheet requires tedious counting of the edge atoms. It is more useful to consider a different procedure that is also helpful in understanding the cone−graphene topology.

DOI: 10.1021/acs.jpcc.6b11350
J. Phys. Chem. C 2017, 121, 1257−1262

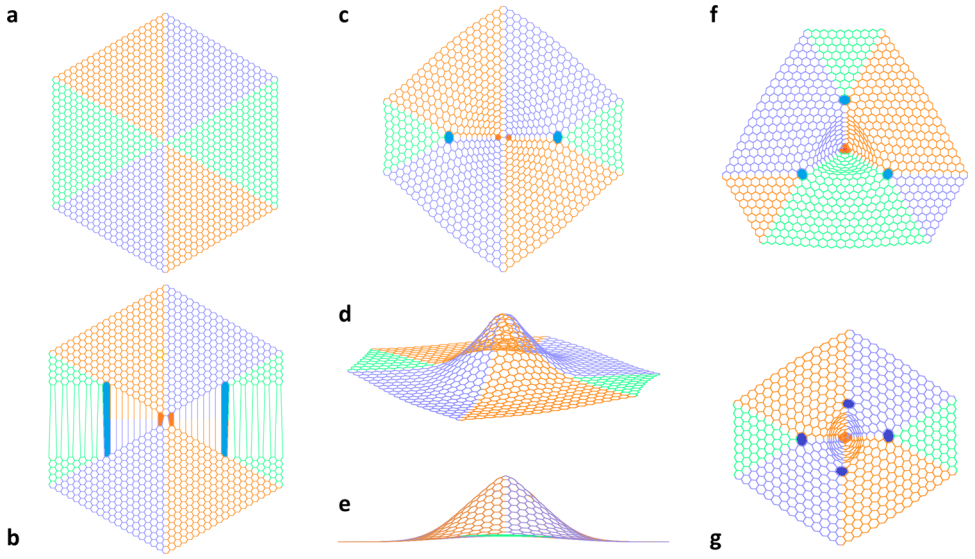

Figure 2. Construction of a cone−graphene junction by removing parts of a graphene sheet. (a) A graphene sheet with six angular sections highlighted. (b) Side graphene sheet with multiple dimer half-lines removed from two sections, the atoms facing each other in the remaining structure are connected subsequently. The pentagons and heptagons are highlighted in orange and light blue, respectively. (c) The cone−graphene structure resulting from geometry optimization of the structure in (b) according to connectivity. (d,e) Side views of the cone−graphene structure of (c). (f,g) various cone−graphene structures, with 3- and 2-fold symmetries, respectively.

In bulk crystals, an edge dislocation is a defect where a half-plane of atoms is introduced midway through the crystal, distorting nearby planes of atoms. In 2D materials such as graphene, an analogous type of dislocation is a point defect where one or several half-lines of atoms is inserted. The most obvious example of the graphene dislocation is the five-seven defect,[27] where a pentagon and a heptagon exist next to each other, and a half-line of atoms is introduced (or taken out, equivalently). If we take a half-ribbon (multiple half-lines) of atoms out of the graphene sheet and "sew up" the remaining geometry, we get a larger dislocation, with the value of the Burgers vector $|\vec{b}| = l$, where l is the distance between the pentagon and the heptagon.

By taking out two half-ribbons from the opposite sides of the graphene sheet, as shown in Figure 2, two dislocations with opposite Burgers vectors are created. Due to the two Burgers vectors canceling out each other, it is actually possible to draw a closed regular hexagonal shape around the two dislocations. In this case, the graphene lattice is not distorted globally, unlike the case of a single dislocation. It is easy to verify that there is a graphitic cone inside the drawn hexagon, in this case with a 4-fold symmetry. Similarly we can obtain cone-graphene structures with N-fold symmetry by cutting out $(6 - N)$ half-ribbons and thus placing $(6 - N)$ dislocations with the total sum of their Burgers vectors equal to zero. Here, N can be 1, 2, 3, or 4.

This construction also shows clearly why a cone with 5-fold symmetry cannot be attached to graphene without causing a global distortion to the graphene lattice. Such a structure requires introducing a single dislocation with a Burgers vector that cannot be canceled out.

Types, Structures, and Topological requirements of NCs. The final step in constructing the NC consists of adding CNTs onto cone−graphene structures. Similar to a regular junction, the total minimum number of heptagons in the NC is also six, as can be shown using the same method. The topological question of interest would be, out of the six heptagons, how many are at the top (where CNT meets cone), and how many are at the bottom (where cone meets graphene).

Since the addition of the CNT does not affect the geometry of the cone−graphene intersection, the number of heptagons at the bottom should stay constant. Therefore, for an NC with a cone of L-fold symmetry, assuming no pentagons, there are $(6 - L)$ heptagons at the bottom, and L heptagons at the top. Note that since we are considering NC with no pentagons, these are the minimum numbers of heptagons in the whole system. If we add in N_5 pentagons to the system, there will be N_5 additional heptagons to pair up with them, so that the total numbers of heptagons and pentagons agree with eq 3. Table 1

Table 1. Topological Make-Ups of NCs

cone symmetry	1	2	3	4
top heptagons	1	2	3	4
bottom heptagons	$N_5 + 5$	$N_5 + 4$	$N_5 + 3$	$N_5 + 2$
bottom pentagons	N_5	N_5	N_5	N_5

lists the possible distributions of heptagons and pentagons in NCs with various cone symmetries; some specific examples of NCs with 2-, 3-, and 4-fold cone symmetries are shown in Figure 3.

Enhanced Thermal Conductivity of NCs. Of all the properties of the pillared architecture with conventional junctions, thermal transport is among the most thoroughly studied. Varshney et al.[19] concluded that "phonon scattering at the CNT−pillar−graphene junctions is the governing mechanism which limit thermal transport in these systems." With geometry being the restrictive factor on thermal transport in junctions, it would be natural to speculate that the NC structure may improve overall heat conductance by providing a smoother shape to reduce phonon scattering.

To explore this possibility, we conducted a series of thermal transport simulations, as described below. We used classical MD, carried out with the package large-scale atomic/molecular massively parallel simulator (LAMMPS).[28,29] Four different

DOI: 10.1021/acs.jpcc.6b11350
J. Phys. Chem. C 2017, 121, 1257−1262

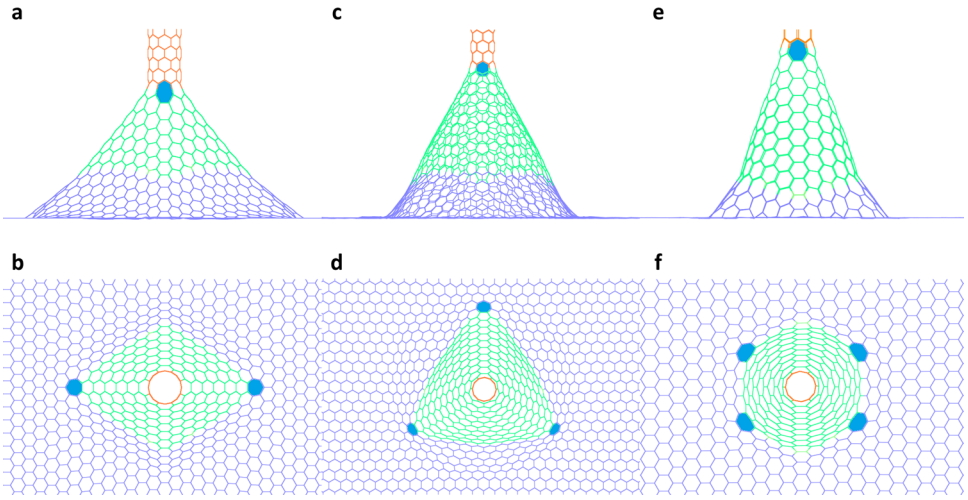

Figure 3. Structures of NCs with different cone symmetry. (a,b) Side and top view of NCs with 4-fold symmetry. (c,d) Side and top views of NCs with 3-fold symmetry. (e,f) Side and top view of NCs with 2-fold symmetry. The symmetry of the cones is not to be confused with the number of heptagons at the base, as we can see the cone of 4-fold symmetry has two heptagons at the base, while that of 2-fold symmetry has four. By symmetry here we are referring to symmetry of atomic connectivity, rather than shapes of the surfaces, which are necessarily distorted to match the components.

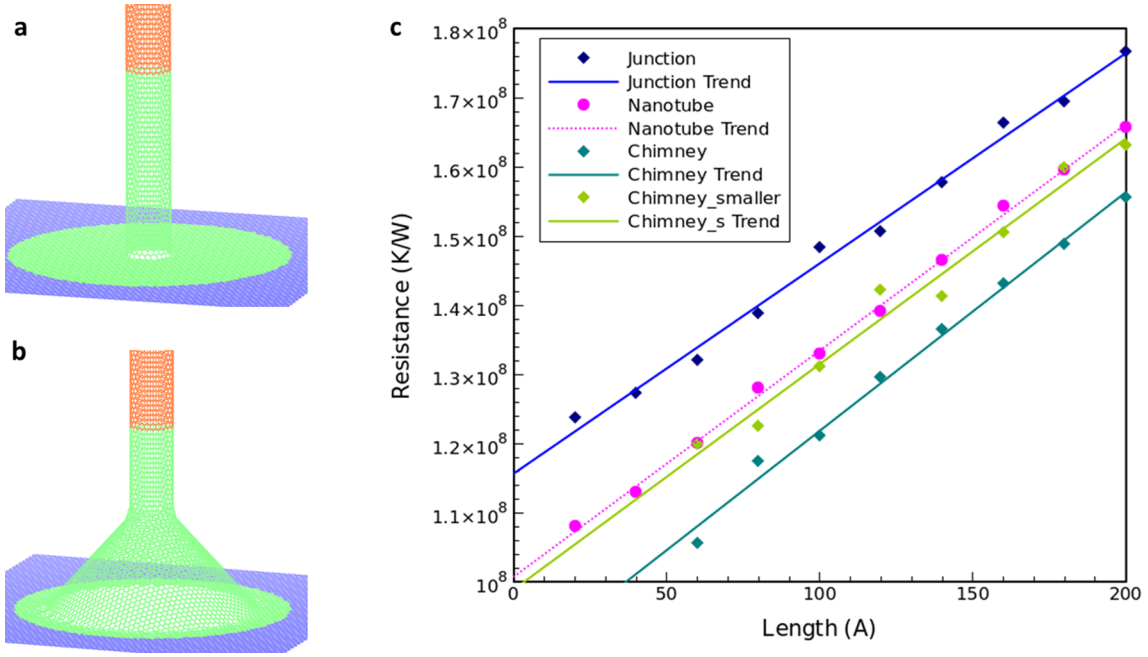

Figure 4. Comparison of thermal properties of different structures: (a) regular CNT−graphene junction, (b) NCs with cones of different sizes and CNT. (c) Calculated thermal resistance of these structures.

structures were designed and measured for thermal resistance: three junctions, in which two were NCs with cones of different sizes, and one regular CNT−graphene junction without cone, and last, one CNT for comparison. The CNTs had a diameter of approximately 20 Å in all calculations. Square graphene sheets were used in all three junctions, with an edge length of about 200 Å. In the two NCs, the cones were 4-fold symmetric topologically and had a slope of 45° with respect to the graphene sheet. The small and large cones in NCs had the base radii of 20 and 40 Å, respectively. The height of the structure, defined as the distance between the center of the graphene sheet and the tip of the CNT, was a variable of our simulation, and ranged between 20 and 200 Å. All four models have approximately 14,000 atoms. The geometries of the regular junction and the NC with a 40 Å cone are shown in Figure 4a,b, respectively.

The thermal transport was simulated by using the heat flux method. The method uses classical molecular dynamics to obtain the heat flux due to nuclear motion. Despite an obvious deficiency of such approach, in graphitic systems it yields thermal conductivities that are comparable with those obtained with full quantum calculations of phonon transport.[32] It does not account for possible electronic conductivity or electron−phonon interactions that can only be captured with ab initio methods.[33] The two ends of the system, as shown in Figure 4a,b in color, were held at two different temperatures using an *NVT* thermostat. The energy added to the hot end is equal to the energy taken from the cold end, and proportional to the

DOI: 10.1021/acs.jpcc.6b11350
J. Phys. Chem. C 2017, 121, 1257−1262

heat flux across the connecting region, namely, the junction. Thus, the thermal resistance is obtained as

$$R = -\frac{\Delta T}{\dot{Q}} \tag{4}$$

Here, R is the thermal resistance of the junction, $\dot{Q}$ is the heat transmitted through the cross-section per unit time, and ΔT is the temperature difference. The resistance is an extrinsic value, as opposed to the intrinsic resistivity. We used the resistance here in order to compare the four test structures with significantly different geometries: two NCs, one regular CNT−graphene junction, and one CNT. The results for the thermal resistance vs height of the structure for all four geometries are shown in Figure 4c.

Our simulations provide a general picture of the thermal behavior of CNT−graphene junctions. With the freestanding CNT as comparison, regular CNT−graphene junction has a resistance that is 20% higher. This hindrance to thermal transmission is caused by the phonon scattering at the connection part of the junctions.[19] Our results, however, show that by adding cones to connect the CNT and graphene components, the NC have enhanced thermal conductance compared to its conventional counterpart. An NC model with a cone radius of 20 Å has a thermal conductance comparable to that of CNT and is 20% more conductive than the regular junction. An NC with a 40 Å cone has a further reduction in thermal resistance by 20%, yielding a value that is lower than that of the regular CNT. As can be seen from Figure 4c, the obtained thermal resistance result does not show fully ballistic patterns. This is likely caused by the limitation of accuracy of the empirical potential-based classical model.[34] This, however, should not affect the relative order of resistances, as they show a common trend with the length of the conductive zone for all structures. The thermal enhancement of NCs as compared to regular junctions is significant, as the connection joints between the CNT "pillars" and the graphene "layers" would be the crucial location of the entire circuit when electrical or thermal flow occurs. The enhancement of thermal transport brought by the NC structures may prove to be yet another step toward future device application of the pillared architecture.[9]

CONCLUSIONS

We have analyzed the geometry and atomistic structure of particular junctions in pillared 3D carbon architectures, termed here nanochimneys (NCs). We find that, under a variety of different shapes and numbers of pentagons/heptagons, there is an underlying constraint for all cone junctions: a minimum requirement of six heptagons, as shown by geometrical consideration. Furthermore, we connect the numbers of heptagons at the top and the bottom of the NC with the symmetry of the cone and demonstrate that, topologically, a cone junction with L-fold symmetry is the equivalent of a cluster of $(6 - L)$ dislocations. Finally, we explored thermal properties of NC, showing that the existence of the cone facilitates the thermal transport of the CNT−graphene junction, pointing to potential device applications, for example, for cooling in micro/nanoelectronics circuits.

AUTHOR INFORMATION

Corresponding Author

*E-mail: biy@rice.edu.

ORCID

Alex Kutana: 0000-0001-6405-6466

Notes

The authors declare no competing financial interest.

ACKNOWLEDGMENTS

Work at Rice University was supported by the AFOSR MURI grant FA9550-12-1-0035 (3D Carbon Networks). Computations were performed on the DAVinCI and Sugar clusters sponsored by funds from NSF grant OCI-0959097.

REFERENCES

(1) Dimitrakakis, G. K.; Tylianakis, E.; Froudakis, G. E. Pillared Graphene: A New 3-D Network Nanostructure for Enhanced Hydrogen Storage. *Nano Lett.* **2008**, *8*, 3166−3170.

(2) Krainyukova, N. V.; Zubarev, E. N. Carbon Honeycomb High Capacity Storage for Gaseous and Liquid Species. *Phys. Rev. Lett.* **2016**, *116*, 055501.

(3) Zhang, Z.; Kutana, A.; Yang, Y.; Krainyukova, N. V.; Penev, E. S.; Yakobson, B. I. Nanomechanics of Carbon Honeycomb Cellular Structures. *Carbon* **2017**, *113*, 26−32.

(4) Paul, R. K.; Ghazinejad, M.; Penchev, M.; Lin, J.; Ozkan, M.; Ozkan, C. S. Synthesis of a Pillared Graphene Nanostructure: A Counterpart of Three-Dimensional Carbon Architectures. *Small* **2010**, *6*, 2309−2313.

(5) Fan, Z.; Yan, J.; Zhi, L.; Zhang, Q.; Wei, T.; Feng, J.; Zhang, M.; Qian, W.; Wei, F. A Three-Dimensional Carbon Nanotube/Graphene Sandwich and Its Application as Electrode in Supercapacitors. *Adv. Mater.* **2010**, *22*, 3723−3728.

(6) Zhang, L. L.; Xiong, Z.; Zhao, X. S. Pillaring Chemically Exfoliated Graphene Oxide with Carbon Nanotubes for Photocatalytic Degradation of Dyes under Visible Light Irradiation. *ACS Nano* **2010**, *4*, 7030−7036.

(7) Lee, D. H.; Kim, J. E.; Han, T. H.; Hwang, J. W.; Jeon, S.; Choi, S.-Y.; Hong, S. H.; Lee, W. J.; Ruoff, R. S.; Kim, S. O. Versatile Carbon Hybrid Films Composed of Vertical Carbon Nanotubes Grown on Mechanically Compliant Graphene Films. *Adv. Mater.* **2010**, *22*, 1247−1252.

(8) Zhu, Y.; et al. A Seamless Three-Dimensional Carbon Nanotube Graphene Hybrid Material. *Nat. Commun.* **2012**, *3*, 1225.

(9) Xue, Y.; Ding, Y.; Niu, J.; Xia, Z.; Roy, A.; Chen, H.; Qu, J.; Wang, Z. L.; Dai, L. Rationally Designed Graphene-Nanotube 3d Architectures with a Seamless Nodal Junction for Efficient Energy Conversion and Storage. *Science Advances* **2015**, *1*, 1400198.

(10) Sihn, S.; Varshney, V.; Roy, A. K.; Farmer, B. L. Prediction of 3d Elastic Moduli and Poisson's Ratios of Pillared Graphene Nanostructures. *Carbon* **2012**, *50*, 603−611.

(11) Guo, S.-J.; Yang, Q.-S.; He, X.-Q.; Liew, K.-M. Design of 3d Carbon Nanotube-Based Nanostructures and Prediction of Their Extra-Strong Mechanical Properties under Tension and Compression. *Comput. Mater. Sci.* **2014**, *85*, 324−331.

(12) Chih-Hao, W.; Te-Hua, F.; Wei-Li, S. Mechanical Properties of Pillared-Graphene Nanostructures Using Molecular Dynamics Simulations. *J. Phys. D: Appl. Phys.* **2014**, *47*, 405302.

(13) Lin, J.; Zhang, C.; Yan, Z.; Zhu, Y.; Peng, Z.; Hauge, R. H.; Natelson, D.; Tour, J. M. 3-Dimensional Graphene Carbon Nanotube Carpet-Based Microsupercapacitors with High Electrochemical Performance. *Nano Lett.* **2013**, *13*, 72−78.

(14) Du, F.; Yu, D.; Dai, L.; Ganguli, S.; Varshney, V.; Roy, A. K. Preparation of Tunable 3d Pillared Carbon Nanotube−Graphene Networks for High-Performance Capacitance. *Chem. Mater.* **2011**, *23*, 4810−4816.

(15) Tylianakis, E.; Psofogiannakis, G. M.; Froudakis, G. E. Li-Doped Pillared Graphene Oxide: A Graphene-Based Nanostructured Material for Hydrogen Storage. *J. Phys. Chem. Lett.* **2010**, *1*, 2459−2464.

(16) Wu, C.-D.; Fang, T.-H.; Lo, J.-Y. Effects of Pressure, Temperature, and Geometric Structure of Pillared Graphene on

DOI: 10.1021/acs.jpcc.6b11350
J. Phys. Chem. C 2017, 121, 1257−1262

Hydrogen Storage Capacity. *Int. J. Hydrogen Energy* **2012**, *37*, 14211−14216.
(17) Li, S.; Luo, Y.; Lv, W.; Yu, W.; Wu, S.; Hou, P.; Yang, Q.; Meng, Q.; Liu, C.; Cheng, H.-M. Vertically Aligned Carbon Nanotubes Grown on Graphene Paper as Electrodes in Lithium-Ion Batteries and Dye-Sensitized Solar Cells. *Adv. Energy Mater.* **2011**, *1*, 486−490.
(18) Novaes, F. D.; Rurali, R.; Ordejón, P. Electronic Transport between Graphene Layers Covalently Connected by Carbon Nanotubes. *ACS Nano* **2010**, *4*, 7596−7602.
(19) Varshney, V.; Patnaik, S. S.; Roy, A. K.; Froudakis, G.; Farmer, B. L. Modeling of Thermal Transport in Pillared-Graphene Architectures. *ACS Nano* **2010**, *4*, 1153−1161.
(20) Lee, J.; Varshney, V.; Brown, J. S.; Roy, A. K.; Farmer, B. L. Single Mode Phonon Scattering at Carbon Nanotube-Graphene Junction in Pillared Graphene Structure. *Appl. Phys. Lett.* **2012**, *100*, 183111.
(21) Pop, E.; Varshney, V.; Roy, A. K. Thermal Properties of Graphene: Fundamentals and Applications. *MRS Bull.* **2012**, *37*, 1273−1281.
(22) Park, J.; Prakash, V. Thermal Transport in 3d Pillared Swcnt−Graphene Nanostructures. *J. Mater. Res.* **2013**, *28*, 940−951.
(23) Bao, H.; Shao, C.; Luo, S.; Hu, M. Enhancement of Interfacial Thermal Transport by Carbon Nanotube-Graphene Junction. *J. Appl. Phys.* **2014**, *115*, 053524.
(24) Li, X.; et al. Large-Area Synthesis of High-Quality and Uniform Graphene Films on Copper Foils. *Science* **2009**, *324*, 1312−1314.
(25) Niu, J.; Li, M.; Choi, W.; Dai, L.; Xia, Z. Growth of Junctions in 3d Carbon Nanotube-Graphene Nanostructures: A Quantum Mechanical Molecular Dynamic Study. *Carbon* **2014**, *67*, 627−634.
(26) Krishnan, A.; Dujardin, E.; Treacy, M. M. J.; Hugdahl, J.; Lynum, S.; Ebbesen, T. W. Graphitic Cones and the Nucleation of Curved Carbon Surfaces. *Nature* **1997**, *388*, 451−454.
(27) Liu, Y.; Yakobson, B. I. Cones, Pringles, and Grain Boundary Landscapes in Graphene Topology. *Nano Lett.* **2010**, *10*, 2178−2183.
(28) Plimpton, S. Fast Parallel Algorithms for Short-Range Molecular Dynamics. *J. Comput. Phys.* **1995**, *117*, 1−19.
(29) Léonard, F.; Tersoff, J. Novel Length Scales in Nanotube Devices. *Phys. Rev. Lett.* **1999**, *83*, 5174−5177.
(30) Stuart, S. J.; Tutein, A. B.; Harrison, J. A. A Reactive Potential for Hydrocarbons with Intermolecular Interactions. *J. Chem. Phys.* **2000**, *112*, 6472−6486.
(31) Ding, F.; Lin, Y.; Krasnov, P. O.; Yakobson, B. I. Nanotube-Derived Carbon Foam for Hydrogen Sorption. *J. Chem. Phys.* **2007**, *127*, 164703.
(32) Singh, D.; Murthy, J. Y.; Fisher, T. S. On the Accuracy of Classical and Long Wavelength Approximations for Phonon Transport in Graphene. *J. Appl. Phys.* **2011**, *110*, 113510.
(33) Penev, E. S.; Kutana, A.; Yakobson, B. I. Can Two-Dimensional Boron Superconduct? *Nano Lett.* **2016**, *16*, 2522−2526.
(34) Muñoz, E.; Lu, J.; Yakobson, B. I. Ballistic Thermal Conductance of Graphene Ribbons. *Nano Lett.* **2010**, *10*, 1652−1656.

DOI: 10.1021/acs.jpcc.6b11350
J. Phys. Chem. C 2017, 121, 1257−1262